REPORT DOCUMENTATION PAGE

Form Approved OMB NO. 0704-0188

1. REPORT DATE (DD-MM-YYYY)	2. REPORT TYPE	3. DATES COVERED (From - To)
17-09-2013	Final Report	18-Jun-2009 - 17-Jun-2012

4. TITLE AND SUBTITLE
NMR Investigation of Atomic Structure and Dynamics of Bulk Metallic Glasses

5a. CONTRACT NUMBER
W911NF-09-1-0343

5b. GRANT NUMBER

5c. PROGRAM ELEMENT NUMBER
8620AK

6. AUTHORS
Yue Wu

5d. PROJECT NUMBER

5e. TASK NUMBER

5f. WORK UNIT NUMBER

7. PERFORMING ORGANIZATION NAMES AND ADDRESSES
University of North Carolina - Chapel Hill
Office of Sponsored Research
104 Airport Drive, Suite 2200, CB #1350
Chapel Hill, NC 27599 -1350

8. PERFORMING ORGANIZATION REPORT NUMBER

9. SPONSORING/MONITORING AGENCY NAME(S) AND ADDRESS(ES)
U.S. Army Research Office
P.O. Box 12211
Research Triangle Park, NC 27709-2211

10. SPONSOR/MONITOR'S ACRONYM(S)
ARO

11. SPONSOR/MONITOR'S REPORT NUMBER(S)
54132-MS.16

12. DISTRIBUTION AVAILIBILITY STATEMENT
Approved for Public Release; Distribution Unlimited

13. SUPPLEMENTARY NOTES
The views, opinions and/or findings contained in this report are those of the author(s) and should not contrued as an official Department of the Army position, policy or decision, unless so designated by other documentation.

14. ABSTRACT
Metallic glasses are amorphous solids consisting of densely packed atoms. Unlike in crystalline solids where point defects and topological defects can be defined unambiguously such as vacancies and dislocations, the structural complexity of metallic glasses makes it rather difficult, for instance, to even describe changes of atomic structures upon mechanical deformation, let alone measure them quantitatively. This makes it extremely challenging to identify experimentally atomic structural changes with certain mechanical properties such as anelastic and plastic

15. SUBJECT TERMS
metallic glasses, NMR, structures, dynamics, glass transition, mechanical properties

16. SECURITY CLASSIFICATION OF:			17. LIMITATION OF ABSTRACT	15. NUMBER OF PAGES	19a. NAME OF RESPONSIBLE PERSON
a. REPORT	b. ABSTRACT	c. THIS PAGE			Yue Wu
UU	UU	UU	UU		19b. TELEPHONE NUMBER: 919-962-0307

Report Title

NMR Investigation of Atomic Structure and Dynamics of Bulk Metallic Glasses

ABSTRACT

Metallic glasses are amorphous solids consisting of densely packed atoms. Unlike in crystalline solids where point defects and topological defects can be defined unambiguously such as vacancies and dislocations, the structural complexity of metallic glasses makes it rather difficult, for instance, to even describe changes of atomic structures upon mechanical deformation, let alone measure them quantitatively. This makes it extremely challenging to identify experimentally atomic structural changes with certain mechanical properties such as anelastic and plastic deformations, a critical step for optimizing mechanical properties of metallic glasses for applications. We demonstrated that, via Al-27 nuclear magnetic resonance (NMR) measurements, that atomic level structures characterized by electric-field-gradient tensors and the electronic properties characterized by the Knight shift-both are sensitive parameters for understanding the mechanical properties of metallic glasses such as the toughness and anelastic deformation. For instance, it was found that the local site symmetry at Al sites measured by NMR changes sensitively under anelastic deformation and there is a strong correlation between hardness and toughness with local electronic properties measured by NMR. These findings established a new approach to understand mechanical properties of glassy metals at atomic scales and could lead to optimized metallic glasses with improved mechanical properties.

Enter List of papers submitted or published that acknowledge ARO support from the start of the project to the date of this printing. List the papers, including journal references, in the following categories:

(a) Papers published in peer-reviewed journals (N/A for none)

Received		Paper
08/31/2011	1.00	X. K. Xi, M. T. Sandor, H. J. Wang, J. Q. Wang, W. H. Wang, Y. Wu. Bonding characters of Al-containing bulk metallic glasses studied by 27Al NMR, Journal of Physics: Condensed Matter, (03 2011): 115501. doi:
08/31/2012	4.00	Magdalena T SANDOR , Laszlo J KECSKES , Qiang HE , Jian XU , Yue WU. Correlation of mechanical properties in bulk metallic glasses with 27Al NMR characteristics, [object Object]Chinese Science Bulletin, (12 2011): 3937. doi:
08/31/2012	7.00	X. K. Xi, M. T. Sandor, J. Q. Wang, H. Y. Bai, W. H. Wang, Y. Wu1. Probing local magnetic cluster development in (CuZr)93-xAl7Gdx bulk metallic glasses by 27Al NMR , Journal of Magnetism and Magnetic Materials, (08 2011): 173. doi:
09/17/2013	9.00	K. Samwer, Y. Wu, H. B. Yu, W. H. Wang. Correlation between beta Relaxation and Self-Diffusion of the Smallest Constituting Atoms in Metallic Glasses, P H Y S I C A L R E V I EW L E T T E R S, (08 2012): 95508. doi:
09/17/2013	15.00	M. T. Sandor, H. B. Ke, W. H. Wang, Y. Wu. Anelasticity-induced increase of the Al-centered local symmetry in the metallic glass La50Ni15Al35, Journal of Physics: Condensed Matter, (04 2013): 165701. doi:
09/17/2013	14.00	X. K. Xi, M. T. Sandor, Y. H. Liu, W. H. Wang, Y. Wu. Structural changes induced by microalloying in Cu46Zr47-xAl7Gdx metallic glasses, Scripta Materialia, (11 2009): 967. doi:
09/17/2013	13.00	M. T. Sandor, X. K. Xi, J. Q. Wang, H. Y. Bai, W. H. Wang, Y. Wu. Probing local magnetic cluster development in (CuZr)(93-x)Al7Gdx bulk metallic glasses by Al-27 NMR, Journal of Magnetism and Magnetic Materials, (01 2012): 173. doi:
TOTAL:	**7**	

Number of Papers published in peer-reviewed journals:

(b) Papers published in non-peer-reviewed journals (N/A for none)

Received		Paper
08/31/2012	5.00	X. K. Xi, J. Q. Wang, H. Y. Bai, W. H. Wang, Y. Wu, M. T. Sandor. Probing local magnetic cluster development in (CuZr)93-xAl7Gdx bulk metallic glasses by 27Al NMR , Journal of Magnetism and Magnetic Materials, (08 2011): 173. doi:
09/17/2013	8.00	M. T. Sandor, H. B. Ke, W. H. Wang, Y. Wu. Anelasticity-induced increase of the Al-centered local symmetry in the metallic glass La50Ni15Al35, Journal of Physics: Condensed Matter, (04 2013): 165701. doi:
TOTAL:		**2**

Number of Papers published in non peer-reviewed journals:

(c) Presentations

Number of Presentations: 4.00

Non Peer-Reviewed Conference Proceeding publications (other than abstracts):

Received	Paper
TOTAL:	

Number of Non Peer-Reviewed Conference Proceeding publications (other than abstracts):

Peer-Reviewed Conference Proceeding publications (other than abstracts):

Received	Paper
TOTAL:	

Number of Peer-Reviewed Conference Proceeding publications (other than abstracts):

(d) Manuscripts

Received		Paper
08/31/2011	2.00	M. T. Sandor1, X. K. Xi, J. Q. Wang, H. Y. Bai, W. H. Wang, Y. Wu. Probing local magnetic cluster development in (CuZr)93-xAl7Gdx bulk metallic glasses by 27Al NMR , Journal of Magnetism and Magnetic Materials (08 2011)
08/31/2011	3.00	M. T. Sandor, L. J. Kecskes, Q. He, J. Xu, Y. Wu. Correlation of mechanical properties in bulk metallic glasses with 27Al NMR characteristics, CHINESE SCIENCE BULLETIN (08 2011)
08/31/2012	6.00	Hai-Bo Ke, Wei-Hua Wang, Yue Wu, Magdalena T. Sandor. NMR observation of anelasticity-induced increase of atomic site symmetry in metallic glasses, Applied Physics Letters (09 2012)
TOTAL:		**3**

Number of Manuscripts:

Books

Received		Paper
TOTAL:		

Patents Submitted

Patents Awarded

Awards

APS Fellow
Kenan Distinguished Professor

Graduate Students

NAME	PERCENT_SUPPORTED	Discipline
Magdalena T. Sandor	1.00	
FTE Equivalent:	**1.00**	
Total Number:	**1**	

Names of Post Doctorates

NAME	PERCENT_SUPPORTED
FTE Equivalent:	
Total Number:	

Names of Faculty Supported

NAME	PERCENT_SUPPORTED	National Academy Member
Yue Wu	0.15	
FTE Equivalent:	**0.15**	
Total Number:	**1**	

Names of Under Graduate students supported

NAME	PERCENT_SUPPORTED
FTE Equivalent:	
Total Number:	

Student Metrics

This section only applies to graduating undergraduates supported by this agreement in this reporting period

The number of undergraduates funded by this agreement who graduated during this period:	0.00
The number of undergraduates funded by this agreement who graduated during this period with a degree in science, mathematics, engineering, or technology fields:.....	0.00
The number of undergraduates funded by your agreement who graduated during this period and will continue to pursue a graduate or Ph.D. degree in science, mathematics, engineering, or technology fields:.....	0.00
Number of graduating undergraduates who achieved a 3.5 GPA to 4.0 (4.0 max scale):	0.00
Number of graduating undergraduates funded by a DoD funded Center of Excellence grant for Education, Research and Engineering:	0.00
The number of undergraduates funded by your agreement who graduated during this period and intend to work for the Department of Defense	0.00
The number of undergraduates funded by your agreement who graduated during this period and will receive scholarships or fellowships for further studies in science, mathematics, engineering or technology fields:	0.00

Names of Personnel receiving masters degrees

NAME
Total Number:

Names of personnel receiving PHDs

NAME
Magdalena T. Sandor
Total Number: 1

Names of other research staff

NAME	PERCENT_SUPPORTED
FTE Equivalent:	
Total Number:	

Sub Contractors (DD882)

Inventions (DD882)

Scientific Progress

Please see attached file

Technology Transfer

Scientific Progress

I. Local magnetism in $(CuZr)_{93-x}Al_7Gd_x$ Bulk Metallic Glasses

Studies of magnetism in metallic glasses have demonstrated overwhelming evidence in support of magnetic inhomogeneities. Structural disorder is extremely influential in metallic glasses giving rise to frustrated magnetic behaviors such as spin-glass, reentrant spin-glass magnetism, and complex cluster-glass states. Anomalous magnetic behaviors in $(CuZr)_{93-x}Al_7Gd_x$ (x = 1, 2) bulk metallic glasses (BMGs) were observed by NMR.

Figure 1.1 shows an example ^{27}Al NMR spectra for x = 2. ^{27}Al is a spin $I = 5/2$ nucleus and, as mentioned in Chapter 2, its spectrum consists of five $|m\rangle \leftrightarrow |m+1\rangle$ transitions including the narrow $|-1/2\rangle \leftrightarrow |1/2\rangle$ central transition, broadened only by the second-order quadrupole effect, and wide satellite transitions $|m\rangle \leftrightarrow |m+1\rangle$ ($m \neq -1/2$) broadened by the first-order quadrupole interactions. Fig. 1.1 shows that the narrow central transition broadens significantly from 1040 ppm at 300 K to 3600 ppm at 77 K. A two-curve Gaussian fit was used to determine the corresponding linewidths of the central and satellite transitions as noted by the dashed curves in Fig 3.1. In addition, the Knight shift of the central transition also changes with temperature. Due to the electronic structure of this metallic glass system, there are two main contributions to the Knight shift $K_{iso} = K_s + K_{s-f}$. K_s is due to the Fermi contact hyperfine interaction associated with the *s* electrons at the Fermi level (as defined in Chapter 2) and K_{s-f} is due to the transferred hyperfine interaction mediated by *s-f* exchange interactions between the localized *f*-electron spins and the spins of *s* electrons. K_{s-f} is given by $A_{hf}\chi_M^f(T)$ where $A_{hf} = zH_{hf}/(N_A\mu_B)$ is the hyperfine coupling constant and is generally assumed to be temperature independent. Here, H_{hf} is the hyperfine field due to local moments, N_A is Avogadro's number, μ_β μ_B is the Bohr magneton, *z* is the number of Gd ions that are nearest neighbors to Al, and $\chi_M^f(T)$ is the bulk magnetic susceptibility due to localized Gd *f* moments.

In general, paramagnetic alloy systems are known to have homogenous magnetic character (i.e. Curie temperature of ~0K, linear isothermal magnetization curves, absence of cusp in AC susceptibility measurements, etc.). Such paramagnetic behavior would be reflected in NMR measurements as a linear dependence of the full-width at half max (FWHM) or linear spectral linewidth on temperature. This would mean that in the case of dipolar or RKKY magnetic interactions the linewidth would be directly proportional to the local time-averaged value of the magnetic moment $\langle S_z \rangle$ as temperature is lowered [58]. Surprisingly, NMR studies of paramagnetic alloy systems $(CuZr)_{93-x}Al_7Gd_x$ for x = 1 & 2 demonstrate a nonlinear linewidth dependence on temperature. Figures 1.2 (a) and (b) below non-linear linewidth broadening commencing at high temperatures.

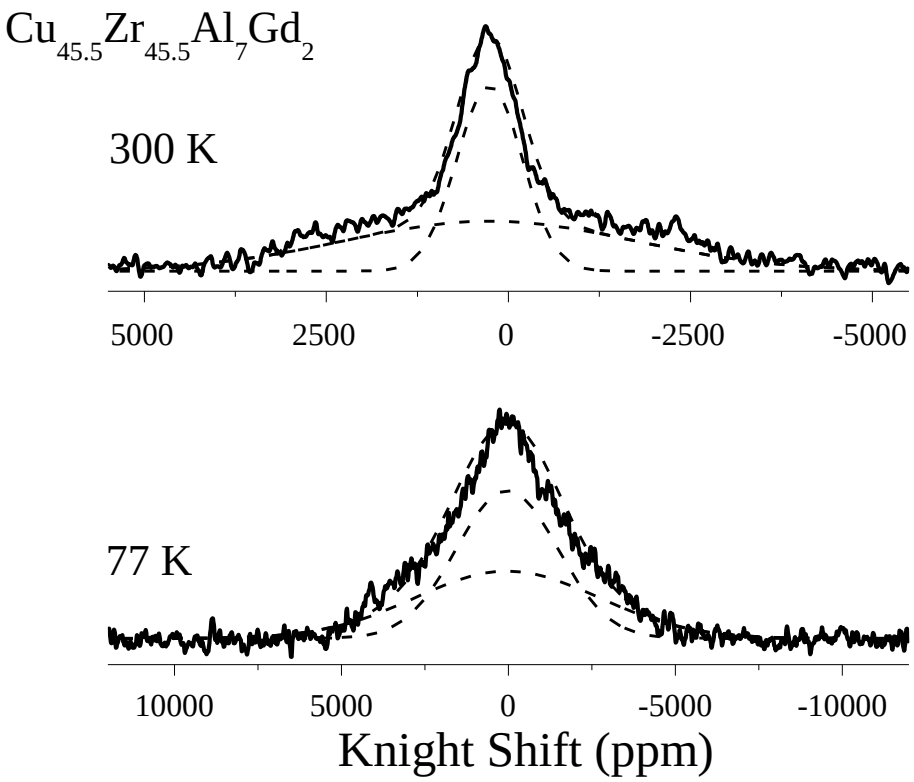

Figure 1.1 NMR frequency shifted spectra for $Cu_{45.5}Zr_{45.5}Al_7Gd_2$ at 300 K and 77 K for comparison. Dashed lines show the two sources of broadening from first-order quadrupole (satellites) broadening and $^{+3}$Gd moments (central transition).

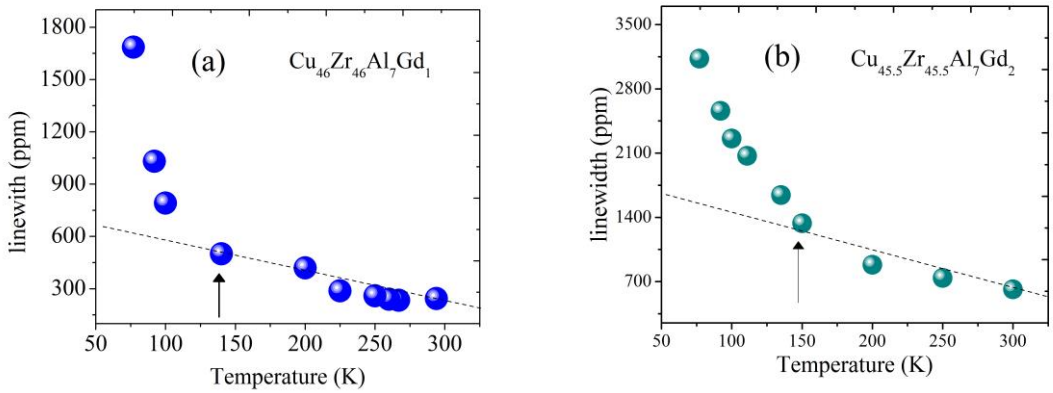

Figure 1.2 (a) & (b) Spectral linewidth for $(CuZr)_{92}Al_7Gd_1$ and $(CuZr)_{91}Al_7Gd_2$. Dashed lines provide a guide for the eye when nonlinear broadening occurs at ~ 150K. Purely paramagnetic alloy systems are expected to display linear linewidth temperature dependence.

The nonlinear behavior shown in Fig. 1.2 can be evaluated within the context of magnetic inhomogeneities. The nature of magnetic inhomogeneities, such as Kondo disorder observed in non-Fermi liquids due to a distribution of magnetic susceptibilities, has previously been evaluated using NMR shift and linewidth data. Assuming A_{hf} and χ are not correlated, the Knight shift can be expressed as an average over all distributions of hyperfine coupling constants and local magnetic susceptibilities

$K = A_{hf}\chi$. Due to the amorphous nature of these BMGs under study, different local environments at ^{27}Al sites are anticipated to induce a spread in susceptibilities and result in nonlinear line-broadening. This line broadening can be evaluated by calculating the experimental fractional NMR linewidth, which is expressed as

$$k / \left|K_{s-f}\right| = \left\{\left[\left(\delta\chi\right)_{rms} / \chi\right]^2 + \left[\left(\delta A_{hf}\right)_{rms} / A_{hf}\right]^2\right\}^{1/2} \qquad (1)$$

where k is the ^{27}Al NMR linewidth. Temperature independent $k/|K_{s-f}|$ values are expected from magnetically homogenous alloys due to spatially independent local susceptibilities and purely paramagnetic systems.

The behavior of line broadening is shown in Figure 1.3 (a) below, which displays data for x = 1 of the ratio $k / \left|K_{s-f}\right|$ versus bulk magnetic susceptibility χ with temperature as an implicit parameter ranging from 77-300 K. Here K_{s-f} was obtained by subtracting the Fermi-contact shift K_s of 342 ppm for x = 1 and 330 ppm for x = 2 as determined from the y-intercept of K_{iso} plotted against χ .This value agrees with the shift value observed in the x = 0 sample ($(CuZr)_{93}Al_7$). In addition, the second-order quadrupole broadening of the central transition was corrected for by subtracting the linewidth found for an x = 0 sample.

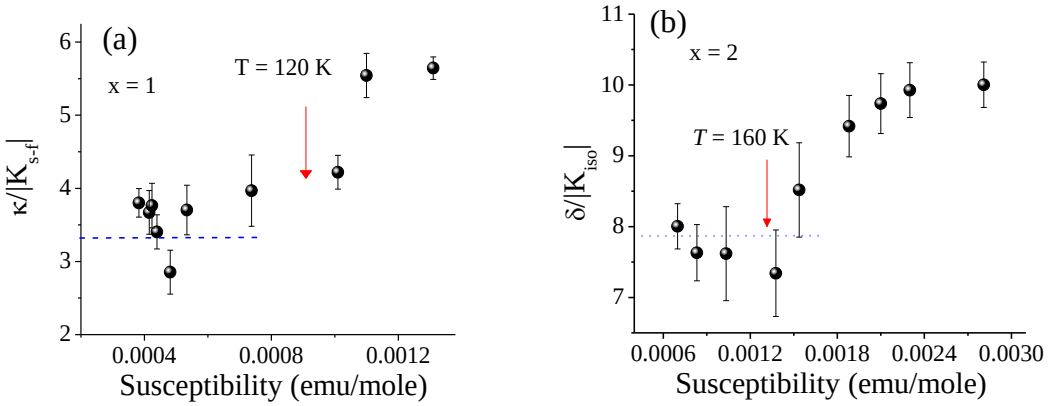

Figure 1.3 k / K_{s-f} versus χ for x = 1 (a) and x = 2 (b) with temperature as an implicit parameter after conduction-electron Knight shift and second order quadrupolar broadening corrections. The dashed lines indicate pure paramagnetic behavior between Gd ions.

The pseudo contact interaction strength was also considered, which results in a dipolar coupling interaction between the thermally averaged magnetic moment of unpaired electrons of a paramagnetic ion and the nucleus. This results in a pseudo contact shift that can be calculated from the distances between the electronic and nuclear spins, which ranged between 3.14 and 3.15 Angstroms. The pseudo contact shifts were found to be negligible giving at most a shift of 4.8 and 9.5 ppm for x = 1 and 2 at 77 K. Fig. 1.3 (a) shows that values of $k / \left|K_{s-f}\right|$ remain constant at high temperatures, as expected for purely

paramagnetic behavior. Near ~120 K the ratio $k/\left|K_{s-f}\right|$ commences proportionality to χ as temperature is lowered. This signifies the onset of a magnetic phase-like transition and supports the existence of a magnetic susceptibility distribution in this temperature regime. In addition, a distribution of A_{hf} is reflected in the large constant offset of ~ 3.5 and is naturally anticipated in amorphous systems. Figure 1.3 (b) displays $k/\left|K_{s-f}\right|$ versus χ for x = 2 and demonstrates a similar NMR linewidth enhancement occurring at a higher temperature of ~ 160 K with a corresponding non-zero distribution of A_{hf} denoted by an offset of ~ 7.75. Anomalies span a wider temperature range for x = 2, which may be due to the twofold increase in the number of magnetic moments. Proportionality between $k/\left|K_{s-f}\right|$ and χ confirms that the linewidth dependence on temperature is significantly stronger than paramagnetic effects caused by RKKY coupling between individual Gd spins and host Al nuclei.

In general, the distribution of susceptibilities and A_{hf} for this alloy system is not entirely unexpected since the spatially disordered nature of these BMGs is anticipated to give rise to a distribution in the magnetic environments due to fluctuations of local interatomic distances and atomic coordination [17]. Interestingly, $k/\left|K_{s-f}\right|$ is observed to saturate near 77K for both compositions and suggests that a magnetic susceptibility distribution develops only over a narrow temperature range between 160-77 and 120-77 degrees for x = 1 and 2, respectively.

The temperature dependence of the hyperfine field A_{hf} is also explored in of Fig. 1.4 (a) and (b) below where K_{s-f} is plotted against χ and shows that A_{hf} is negative as evidenced in the slope. A linear fit was applied yielding a transferred hyperfine field of $zH_{hf} = -1.2$ kOe for x = 1 and $zH_{hf} = -0.6$ kOe for x = 2. A distribution in A_{hf} and χ mentioned previously would suggest that these couplings might have various strengths in temperature and space. The linear behavior demonstrated in both x = 1 and x = 2 shows that A_{hf} is temperature independent and is not the source of non-linear NMR linewidth broadening in the temperature range of 77-300 K.

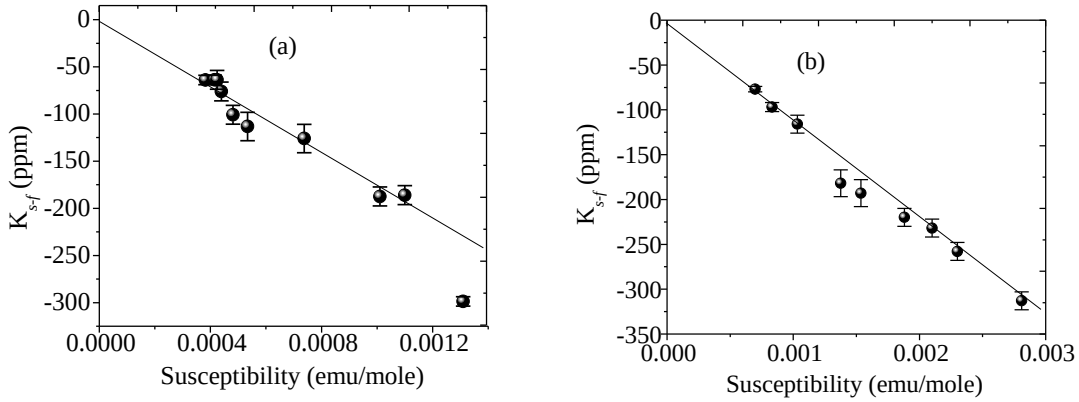

Figure 1.4 for x = 1 (a) and x = 2 (b) displays K_{s-f} versus χ with temperature as an implicit parameter. The behavior of A_{hf} is inferred from the slope.

In general, NMR and magnetization measurements both confirm the development and the importance of AF short-range order for $(CuZr)_{93-x}Al_7Gd_x$ glasses x = 1 and 2, beginning at high temperatures near 150K. This is supported by temperature-independent hyperfine couplings A_{hf} for x = 1 and x = 2 that show the source of broadening is due to the local magnetic susceptibility distribution at high temperatures. Non-linear linewidth broadening clearly proves that this distribution is prominent at high temperatures, evolves over a narrow temperature range (40-80 degrees). Furthermore, non-Brillouin isothermal magnetization behavior at low temperatures seems to suggest that the AF cluster development in both x = 1 and 2 is magnetically frustrated. The intra-cluster interaction strength for x = 1 and 2, as determined by the exchange integral $\left|J_{s-f}\right|$, shows that this frustration is quite strong as it is considerably higher than other Gd-bearing amorphous systems showing long-range spin-glass behavior.

II. Anelastic deformation of La-based metallic glass

One of the great challenges in the study of bulk metallic glasses (BMGs) is a basic understanding of the deformation mechanism where in amorphous systems dislocation is absent. Plastic flow in metallic glasses can proceed by two mechanisms: inhomogenous and homogenous deformation. Inhomogenous deformation takes place at low temperatures and high stresses resulting in highly localized shear banding (at 45° with respect to the tensile axis), since only a small fraction of the volume sample participates in flow. At low stress and higher temperatures (near T_g) the entire volume sample can undergo homogenous deformation [20]. These two mechanisms showing macroscopic deformation are illustrated in Figure 4.1. The strain response during homogenous deformation exhibits both elastic and inelastic (anelastic and viscoplastic) strain components where the elastic strain recovers instantaneously, the anelastic strain undergoes time-dependent recovery, and the viscoplastic strain is permanent. This can be compared to crystalline systems, where plastic flow occurs by propagation of dislocations or line defects that have a definite slip plane. This Chapter will focus on using NMR to understand homogenous deformation of anelastic deformation.

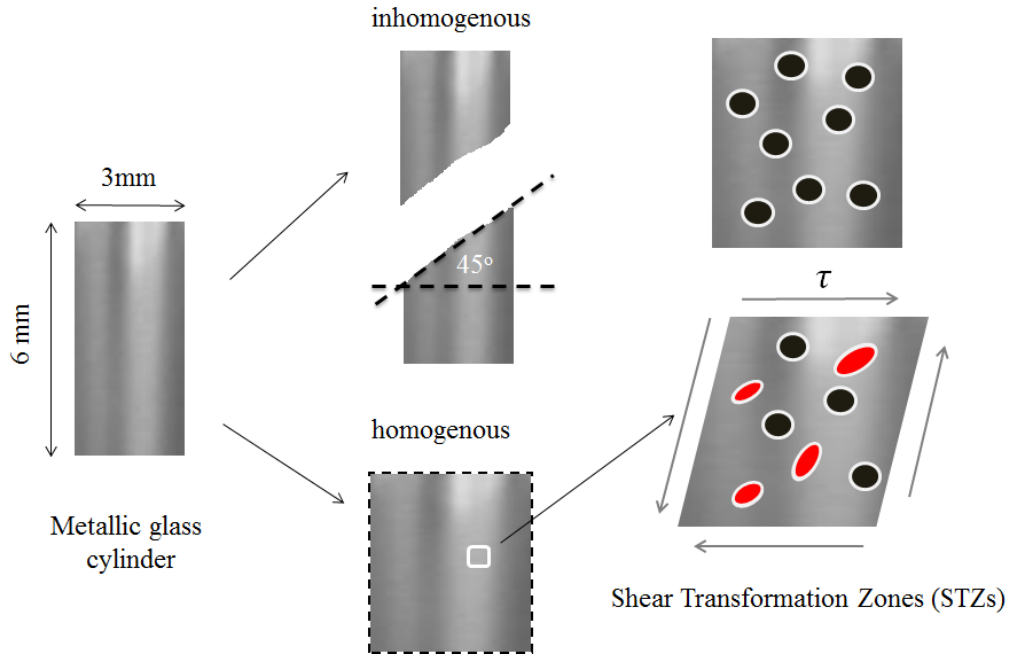

Figure 2.1 Schematic illustrating the two deformation mechanisms observed in metallic glasses. Shear transformation zones (STZs) correspond to the regions of local atomic rearrangements that take place during a shear.

Phenomenological models of inelastic deformation describe the fundamental flow mechanism in metallic glass as a process involving a local atomic rearrangement of atoms that accommodates strain though single atomic diffusion or as a cooperative shear process of atomic clusters referred to as shear-transformation zones (STZs). This is also illustrated in Fig. 2.1. These deformation mechanisms are believed to be facilitated by a distribution of free volume that is a widely used scalar parameter for quantifying structural relaxation and creep kinetics in metallic glass. Free volume is defined as the volume that is in excess of the material's corresponding crystalline state or ideally ordered structural state. The red highlighted areas in Fig. 2.1 represent STZs that are in close proximity to regions of large free volume and therefore, can easily undergo shear. Due to the amorphous nature of metallic glass, there is believed to be a continuous distribution of different local structure and free volume. In essence, this is what makes up the defects in metallic glass.

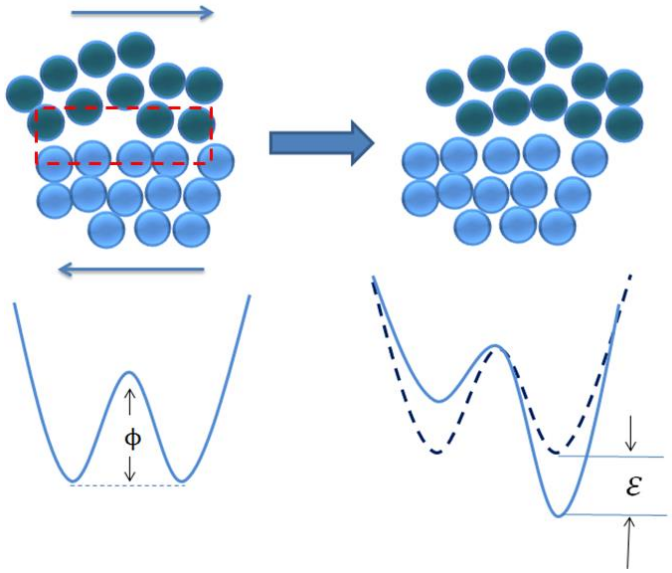

Figure 2.2 At the atomic-level, local regions of metallic glass have symmetric free energies ϕ. Applying a stress lowers the free energy by ε in the direction of shear and causes atomic rearrangements.

Deriving an understanding of how the local structure/free volume evolves under shear stress might provide tremendous insight into the deformation mechanism in metallic glass. Currently, anelastic and viscoplastic deformations of metallic glasses are mostly interpreted in terms of STZs. As shown in Figure 2.2, the distribution of structure and free volume in glass gives rise to local free energies ϕ that are approximately symmetrical. The application of shear stress induces an asymmetry of the local free energy by an amount ε and causes mechanical polarization of STZs. This effectively increases the probability for atoms to reshuffle along the direction of shear. Backward atomic shuffling is possible, but has a much lower probability.

During an applied stress local regions that are sheared are not isolated. STZs are embedded in an elastic surrounding that exerts a back stress on the transformed volume. The backstress developed during anelastic deformation is anticipated to aide in the macroscopic recovery of the shape when the applied stress is released. This gives rise to delayed-elastic or anelastic recovery. Previous studies have shown

that the anelastic recovery of glass exhibits a continuous spectrum of activation energies and relaxation times reflecting the resulting distortion of free volume and local structural distribution due to STZs. If two or more neighboring transformed STZs emerge and interact with each other, dissipative release of the back stress could occur resulting in viscoplasticity. This chapter will cover the anelastic response of La-based metallic glass due to constant compression experiments at room temperature.

For constant compression experiments, $La_{50}Ni_{15}Al_{35}$ BMG rods 3mm in diameter and ~6 mm length were prepared by arc-melting the elemental components under a Ti-gettered argon atmosphere. A cylinder, 3 mm in diameter and 50 mm long, was cast in a water-cooled copper mold. The samples to undergo constant compression experiments were cut from the middle of the cylinder by a diamond saw, and the ends of the samples were carefully polished flat and normal to the longitudinal axis for uniform loading in compression. It was recently found that homogenous deformation of metallic glass rods at room temperature could be obtained at high stress by applying a stress just below the yield strength. As a result, the samples were compressed at a strain rate of $1\times10^{-4}s^{-1}$ (Instron electromechanical testing system 3384) to a stress equal to .90 of the metallic-glass yield strength ($\sigma = 900\ Mpa$), and held at this stress for 10, 24, and 48 hours. The effect of different stress was also explored by studying rods that were compressed for 24 hours at a stress equal to .80 ($\sigma = 800\ Mpa$) and .90 ($\sigma = 900\ Mpa$) of the metallic-glass yield strength. The amorphous nature of these BMGs was confirmed using DSC and x-ray diffraction. An as-cast rod (no mechanical treatment) and annealed rod at T_g – 20 (240 °C) degrees for 48 hours were used as reference samples. Figure 2.3 shows an example of a strain curve for constant compression at room temperature for 24 hours. The strain response is characterized by three components: elastic (~ 1.90%), anelastic (~.10%), and a sum of viscoplastic and anelastic (~.04%) components. It is important to note that anelastic strain continues even at the onset of viscoplastic strain.

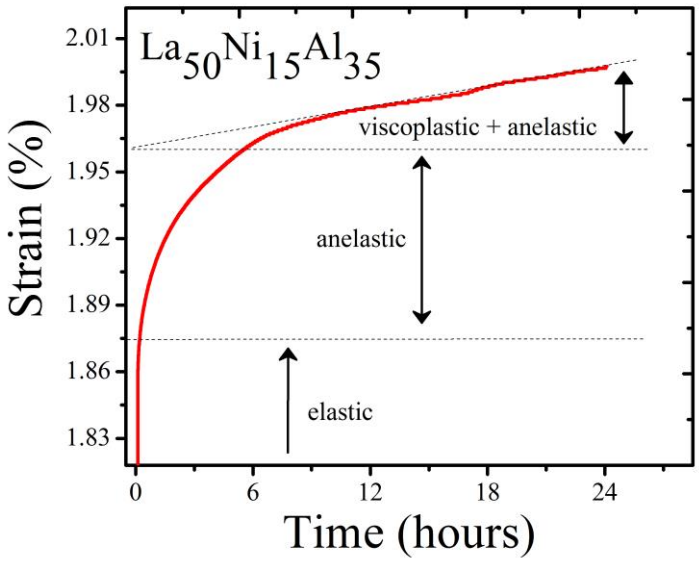

Figure 2.3 (a) Room temperature creep experiments for 24 hours. The elastic (~1.90%), anelastic (~.10%) (delayed elastic), and anelastic and viscoplastic strain (~.04%) responses are noted.

Figure 2.4 shows ^{27}Al NMR nutation profiles of the central transition intensity versus the width of the first pulse t_1 ranging from 0 to 6.5 μs for as-cast, annealed, and compressed $La_{50}Ni_{15}Al_{35}$ BMG

samples. ^{27}Al is a spin $I = 5/2$ nucleus and permits coupling between the electric quadrupole moment and the EFG due to quadrupole interaction. For weak perturbation of the Zeeman interaction the intensity represents evolution of the density operator $\rho(t_1, \tau_1, t_2, \tau_2)$ due to first-order quadrupole interactions. The fitting parameter $\omega_Q = \frac{3e^2qQ}{2I(2I-1)\hbar}$ provides direct determination of the EFG reflecting any local compression-induced structural changes. The EFG experienced at ^{27}Al sites is most sensitive to the position the aluminum atom's nearest neighbors and is negligible in instances of high symmetry, e.g., cubic, icosahedral order, etc.

Fits of the nutation curves are shown as solid lines in Fig. 2.4 for an asymmetry parameter η of .9 and the extracted values of ω_Q are listed in Table 2.1 with the corresponding strain changes. Complete anelastic recovery of strain is observed for a compression time of 10 hours and, results in a decrease of ω_Q from 820 to 615 kHz compared to the as-cast samples. A decrease in ω_Q corresponds to a reduction of the largest principle component of EFG tensor, V_{zz}. This provides direct experimental evidence that anelasticty is responsible for the structural changes induced locally at Al sites. Fit values of ω_Q also decrease to 653 kHz for 24 hours and 528 kHz for 48 hours of strain time. This demonstrates that anelastic-induced structural changes are proportional to compression time thereby enhancing the local symmetry at ^{27}Al sites. Annealing for 48 hours below T_g gives a

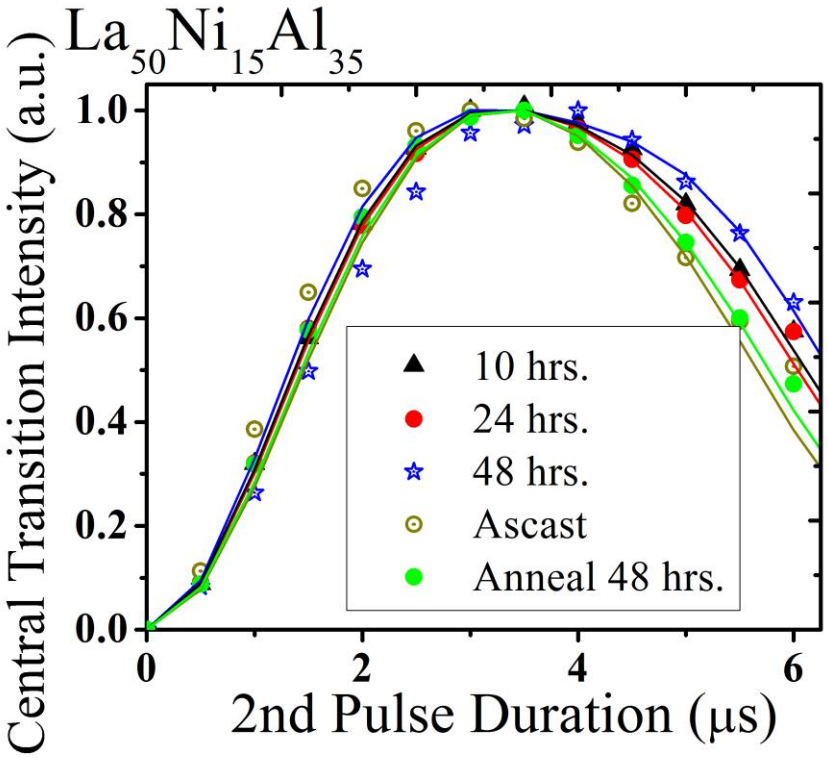

Figure 2.4: Nutation experiments where the central transition intensity is plotted versus the second pulse duration in a Hahn-echo sequence. The pulse duration t_1 increases from 0 to 6.5 μs by steps of 0.5 μs. Solid lines are fittings of ω_Q and summarized in Table 4.2 in addition length change percentages.

ω_Q of 765 kHz and shows that local site symmetry is slightly enhanced although to a much lesser degree than by compression.

Figure 2.5 shows nutation experiments for compressed samples demonstrating complete structural relaxation after a 1 month period. These results are summarized with the nutation data of the as-cast and annealed samples and a nutation curve fit parameter of $\omega_Q = 810$ kHz for comparison. This clearly supports that for large applied stresses the residual backstress developed during anelastic deformation promotes not only the fast macroscopic recovery of the shape, which is comparable to the timescale of the experiment, but also causes relaxation of the slower anelastic-induced local structural changes that exceeds the duration of the experiment.

Table 2.1. Fitting values of quadrupole frequency $\omega_Q / 2\pi$, length changes, and Knight shift values (ppm).

$La_{50}Ni_{15}Al_{35}$ (Fig 4.6)	$\omega_Q / 2\pi$ (kHz)	% Length Change	Knight Shift (ppm)
As-cast	820	-	657
10 hrs.	615	0.0%	657
24 hrs.	653	-0.03%	657
48 hrs.	528	-0.04%	657
Anneal – 48 hrs.	765	-.09%	647
As-cast (Fig. 4.7)	700	-	657
800 Mpa	615	-0.03%	657
900 Mpa	562	-0.03%	657

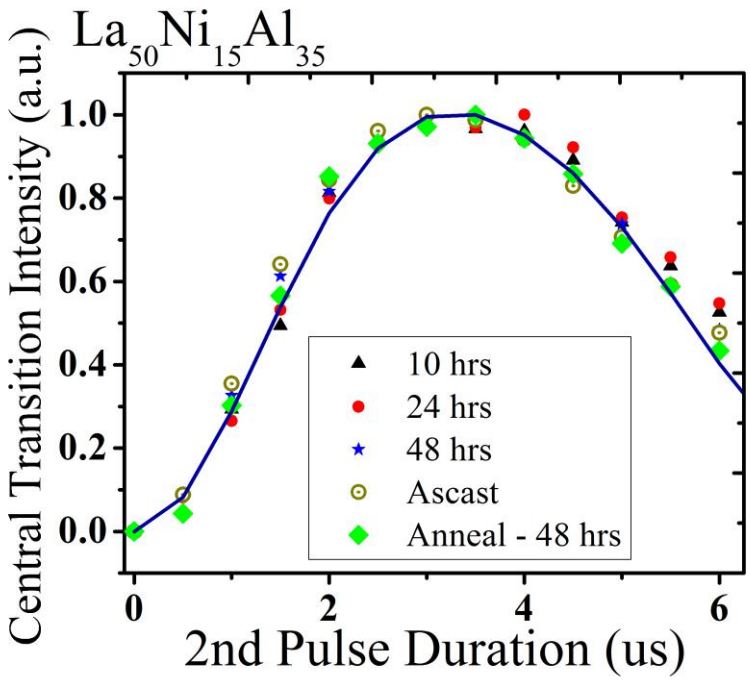

Figure 2.5: Nutation experimental data for as-cast, compressed, and annealed samples (data points), which show no changes in structural symmetry due to anelastic relaxation for ~ 1 month. The fit of the nutation curve gives ω_Q=810 kHz.

Changes of electronic structure exhibited through annealing and anelastic-induced site symmetry probed by NMR can be reconciled within the theory of atomic-level stresses and site symmetry coefficients. According to this theory, the stress state of an amorphous structure can be considered when a small strain $\vec{r}$ is applied yielding a change in the total internal potential energy by $\Delta E_i = \frac{1}{2}\sum_{\alpha\beta}\sigma_i^{\alpha\beta}\varepsilon^{\alpha\beta}$. $\varepsilon^{\alpha\beta}$ and $\sigma_i^{\alpha\beta}$ are second-rank tensors that define components of applied strain and atomic-level stress, respectively. Two relevant quantities that are derived from the change of energy ΔE_i are the hydrostatic pressure p and local average shear stress τ . Additional local parameters such as site symmetry coefficients can be obtained by expressing the change of potential energy as an expansion of spherical harmonics by $\Delta E = \sum_n \varepsilon_n^{l,m}(i) Y_l^m(\theta_i,\varphi_i)\frac{|r_i|^n}{n!}$. The site symmetry coefficients are given by $\alpha_o = \varepsilon_2^{0,0}$ $(l=0)$ and $\beta = \sqrt{\left(\sum_{m=-2}^{2}|\varepsilon_2^{2,m}|^2\right)}\alpha_o^{-1}$ $(l=2)$, where α_o is a measure of the average harmonic potential energy curvature directly correlated to the atomic volume or hydrostatic pressure p, and β is related to the deviation of spherical symmetry that is associated with the local shear stress, τ .

The change of potential energy ΔE_i due to atomic-level stresses directly parallels the change of quadrupole coupling energy given by $\Delta E_i = \frac{1}{6}\sum_{\alpha\beta}V_i^{\alpha\beta}Q^{\alpha\beta}$ where $Q^{\alpha\beta}$ defines the quadrupole moment

tensor and $V_i^{\alpha\beta}$ is the second-rank EFG tensor that is probed by the best fit parameter ω_Q of NMR nutation experiments. Since $Q^{\alpha\beta}$ is an intrinsic property of the NMR probe nucleus $V_i^{\alpha\beta}$ provides a strong correspondence to $\sigma_i^{\alpha\beta}$. Given the physical importance of p and τ, analogies can also be made between site symmetry coefficients and properties measured by NMR. Anelastic-induced structural changes in Fig. 2.4 probed by ω_Q is equivalent to the $l = 2$ coefficient and the distribution of local shear stress τ. Similarly, the symmetry coefficient $l = 0$ directly coincides with the changes of local electric structure due to annealing that gives rise to a smaller Knight shift (647 ppm). Numerical studies indicate that fluctuations of local shear stress τ are independent of changes of hydrostatic pressure, *p*. This agrees with the negligible changes of NMR knight shift and free volume due to anelastic compression. Within the theoretical framework of atomic level stresses, NMR nutation and spectroscopy results provide evidence to suggest that the mechanism of anelastic deformation is one that causes local shear rearrangements of atoms that not only enhances local site symmetry, but to also lowers the change in internal potential energy by minimizing the local distribution of atomic-level stress. This suggests that local shearing of atoms is accommodated by approaching a more ideal structural state.

In conclusion, ^{27}Al NMR and MDSC studies of $La_{50}Ni_{15}Al_{35}$ were utilized to provide a snapshot of anelastic-induced structural changes that were compared with as-cast and annealed reference states. The data reveals that anelastic strain causes an increase in local symmetry near Al atoms that is proportional to compression time whereas the corresponding changes of free volume were negligible due to the small viscoplastic strain. It was also shown that these anelastic-induced changes occur everywhere throughout the glass and have a relaxation timescale that is long compared the duration of the constant compression experiments. Furthermore, it was observed that local changes of electronic structure are closely linked to fluctuations of the local density obtained through annealing. The results here show that anelastic deformation mechanism can be described within the theory of atomic level stresses.

III. Correlation of electronic properties and mechanical properties

In this study, Zr-based BMGs ($Zr_{56}Co_{28}Al_{16}$, $Zr_{60}Ni_{21}Al_{19}$, $Zr_{48}Cu_{45}Al_7$, $Zr_{60}Cu_{28}Al_{12}$, and $Zr_{61}Ti_2Cu_{25}Al_{12}$), and ZrHf-based BMGs ($(Zr_{1-x}Hf_x)_{52.5}Ti_5Cu_{17.9}Ni_{14.6}Al_{10}$ from x = 0.0 to 1.0) were investigated due to their good GFA and favorable mechanical properties such as toughness and hardness. ^{27}Al NMR experiments were performed at room temperature in a magnetic field of 8.89 T. NMR spectra were acquired using a Hahn-echo pulse sequence. Magnetization measurements were also conducted using a Quantum Design SQUID magnetometer. The magnetization of metallic glass samples were measured as a function of varying field from 50,000 to -50,000 Oe in steps of 5,000 Oe.

Figures 3.1(a) and (b) show ^{27}Al NMR spectra for Zr-based and ZrHf-based BMG samples, respectively. Changes of the local electronic states at Al sites are clear based on the systematic changes of spectral shift caused by variations of both the aluminum and transition metal (Zr, Cu, Ni, Co, Ti) content (Fig. 3.1 (a)) and also by systematic variation of the Hf/Zr ratio with fixed aluminum content (Fig. 3.1 (b)). The dominant shift mechanism for metallic systems is given by the Knight shift K_{iso}, which is the direct contact shift due to the Fermi contact hyperfine interaction associated with the Pauli susceptibility χ^s_{Pauli} of *s* electrons at the Fermi level. The values of the Knight shift given in Fig. 3.1 (a) and (b) are on the order of ~350 ppm demonstrating that the *s*-electron contribution at the Fermi energy is quite small as compared to the shift in pure Al metal (~1630 ppm). This is consistent with recent electronic structure calculations of Al-Zr-Cu and Al-Ca amorphous systems. The calculations indicate that the *s*-electron band is significantly

shifted to higher binding energies whereas the valence *d*-electron band of transition metals remain prominent at the Fermi level.

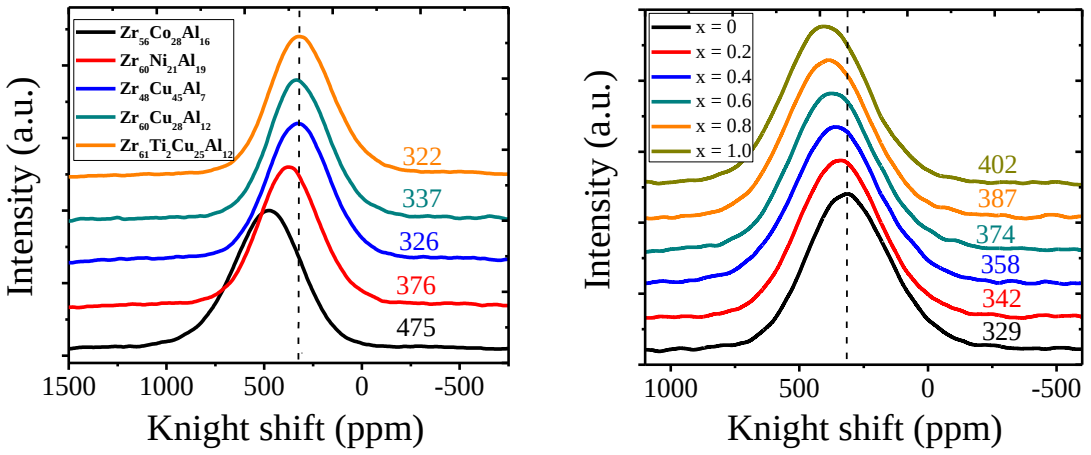

(a) (b)

Figure 3.1: (a) Room temperature ^{27}Al NMR spectra for $Zr_{56}Co_{28}Al_{16}$, Zr_{60} Ni_{21} Al_{19}, $Zr_{48}Cu_{45}Al_7$, $Zr_{60}Cu_{28}Al_{12}$, and $Zr_{61}Ti_2Cu_{25}Al_{12}$ BMGs. (b) Room temperature Al NMR spectra for $(Zr_{1-x}Hf_x)_{52.5}Ti_5Cu_{17.9}Ni_{14.6}Al_{10}$ BMG system from x = 0 to 1.0 .

Correlations of hardness and toughness with the ^{27}Al Knight shift K_{iso} values are displayed in Fig. 3.2. These results show that the local electronic structure at Al sites correlate with the hardness and toughness properties of BMGs. Figure 3.2 (b) shows linear correlation between the hardness and the ^{27}Al Knight shift, where the Zr/Hf ratio is an implicit parameter. Figure 3.2 (a) shows that the toughness decreases with increasing ^{27}Al Knight shift K_{iso} although the correlation is not linear and is weak. In order to make further understanding magnetic susceptibility is measured.

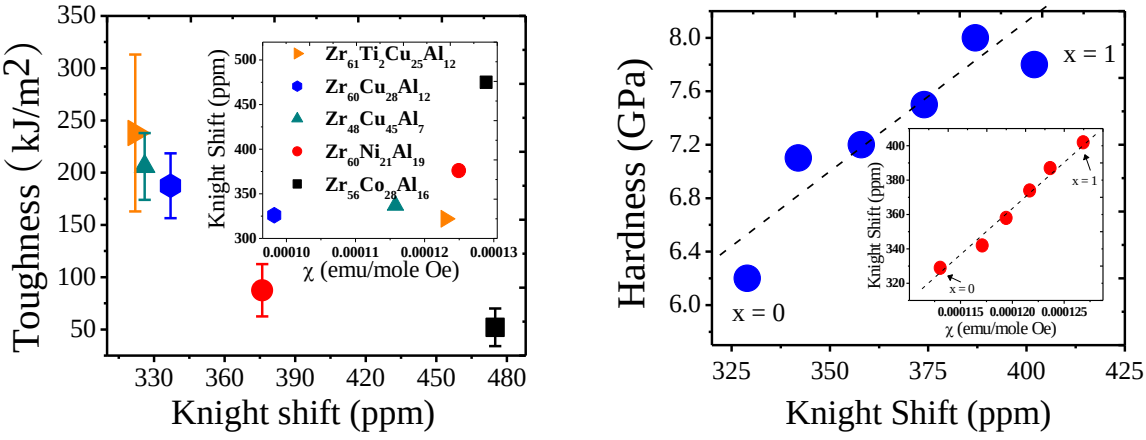

(a) (b)

Figure 3.2: (a) Toughness (kJ/m^2) properties are plotted as a function of Knight shift K_{iso} for Zr-based BMGs demonstrating a direct correlation between mechanical properties and local electronic structure. (b) Hardness (GPa) properties of ZrHf-based BMGs are plotted versus the Knight shift K_{iso} showing a

systematic correlation. The insets of both figures display the corresponding correlation between the Knight shift K_{iso} and the total magnetic susceptibility $\chi_{\exp} - \chi_{core}$.

The insets of Figure 3.2 (a) and (b) display a direct correlation of total magnetic susceptibility $\chi_{\exp}$ with K_{iso}. The total measured magnetic susceptibility for each composition was corrected for by a weighted average of the diamagnetic core susceptibilities. The total susceptibility can be further expressed as $\chi_{\exp} - \chi_{core} = \chi^{s}_{Pauli} + \chi_{L} + \chi^{d}_{Pauli} + \chi_{orb}$, where χ_{L} is the Landau diamagnetic *s*-conduction electron susceptibility. Except for χ_{orb}, all contributions to the total susceptibility are directly related to the *s* or *d* electronic density of states (DOS). The *d*-electron contribution $\chi^{d}_{Pauli} + \chi_{orb}$ of the total susceptibility can be approximated by subtracting the free *s*-conduction contribution $\chi^{s}_{Pauli} + \chi_{L}$ from the total measured susceptibility. The dependence of toughness and hardness properties on *d*-electron susceptibility is demonstrated in Figure 3.3. One should note that $Zr_{56}Co_{28}Al_{16}$ does not fit into this trend and can be attributed to the susceptibility contribution caused by χ_{orb} due to a nearly half-filled *d*-band of Co, which is otherwise negligible in the other compositions.

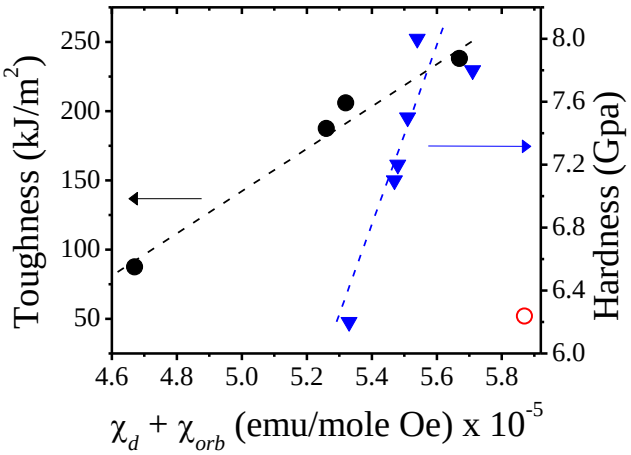

Figure 3.3: Toughness (●) and hardness (▼) properties for Zr and ZrHf-based BMGs are plotted versus $\chi_d + \chi_{orb}$ from Table 1 showing an approximately linear correlation. The outlier of the trend seen here is from $Zr_{56}Co_{28}Al_{16}$ due to enhanced χ_{orb} and is noted with a different symbol (○).

This work provides insight into the correlations that exist between both the local electronic structure at Al sites and magnetic susceptibility with hardness and toughness properties of Zr and ZrHf-based BMGs. The experimental data presented here clearly provides evidence that for transition metal-based BMGs, the *d*-electron structure is very important for obtaining favorable mechanical properties. The correlations observed in this study provide a guide for designing BMGs with specific mechanical properties of interest.